Interaction of fundamental Lamb modes with a point impact damaged zone in composite plates

Dilbag Singh, Rachid El Guerjouma, Mourad Bentahar

ACOUSTICS 2012

Interaction of fundamental Lamb modes with a point impact damaged zone in composite plates

D. Singh, R. El Guerjouma and M. Bentahar

Laboratoire d'acoustique de l'université du Maine, Bât. IAM - UFR Sciences Avenue Olivier Messiaen 72085 Le Mans Cedex 9
kahlondilbag@yahoo.com

Due to high specific strength and stiffness for low weight, composite materials are increasingly used in aerospace, naval, and automotive applications these days. However, one weakness of such materials is their sensitivity to impacts, which may cause severe and harmful damages. In this paper, we have studied numerically the interaction behaviour of fundamental A_0 Lamb mode with the damaged zone caused due to a point impact on the surface of the composite plate. A 3-Dimensional finite element model is used to simulate the scattering phenomenon of fundamental A_0 incident Lamb mode sent towards the damaged zone. The damaged zone inside the composite plate has been modeled as a conical shaped geometry with decayed material stiffness properties. The directivity pattern of the scattered field for the A_0 Lamb wave mode is predicted from the 3D finite element simulations and plotted graphically for different positions and geometrical size of the defect. These results may provide the basis for the quantification of the detection sensitivity for impact zones in composite plates using guided wave sensors.

1 Introduction

In recent years, the use of composite materials has increased exponentially in several aerospace, naval, and automotive applications due to their high specific strength and stiffness for low weight. However, composite materials have a serious weakness of sensitivity to impacts, which may cause severe and harmful damages while being barely visible. Impact events can be produced by tool drops during the manufacturing, preparation or storage of the structure, or during in-service use, e.g., birds collisions for aeronautic components, hail impact and so on. Impact damages may not be visible from the surface of the material, and even so, small scratches at the surface may hide severe damages underneath, inside the medium, like matrix cracking, fibers failure and/or delamination between plies. The cause of such damage is usually the shock wave, which is produced during the impact and propagates mechanical energy deep inside the material, thus causing breaking along its path. Since it is difficult to avoid accidents, it is very necessary to reliably detect and evaluate impact damages, as well as their effects on residual resistance of the structure. Meanwhile, it is also well-known that mechanical properties of composite materials can be severely degraded by the initiation and propagation of structural damages (fiber breakage, delamination, matrix cracking...), which may appear during the components life cycles. If impacts can locally cause crack-like defects similar to those mentioned above, they also may lead to local decays in material properties, i.e., in the vicinity of the impacted zone [1].

In this paper, we investigate numerically the propagation of ultrasonic guided wave mode along plate-like structures, and their scattering by a cracked zone being representative of impact damage. Because of the angular spreading of the shock wave produced by a point impact, the shape of impact damages is usually conical, the tip head being at the plate surface, precisely where the impact happens. A 3-Dimensional frequency domain Finite Element model is used to simulate the scattering phenomenon of fundamental incident Lamb A_0 mode sent towards the damaged zone. The damaged zone inside the composite plate has been modeled as a conical shaped geometry with decayed material stiffness properties. The frequency of the incident Lamb mode is chosen to be below A_1 cut-off. The directivity pattern of the scattered field for the A_0 Lamb wave modes are predicted from this 3D Finite Element simulations for two different positions of the impact zone. The effect of different geometry size as radius of base and height of the conical shape is also shown graphically. A conclusion of the study is presented at the end of the article.

2 3-Dimensional Finite Element model for anisotropic materials

To simulate the dynamic responses of viscoelastic, anisotropic plates in 3D, a commercially available numerical analysis package [2] based on the finite element method is used in our study. Besides, one external routine is developed for getting the normal displacements of the scattered field around the point impact at circular positions after the FE model is solved in computer.

In the FE model, the equation of dynamic equilibrium for orthotropic viscoelastic material (with nine complex moduli) is written and solved in the Fourier domain as

$$\sum_{j,k,l=1}^{3} C_{ikjl}\left[\frac{\partial^2 u_j}{\partial x_k \partial x_l}\right] + \rho\omega^2 u_i = 0,\ i = 1,2,3, \quad (1)$$

where u_i is the Fourier transform of the components of the displacement vector $\boldsymbol{u}$, with i = 1, 2, 3 representing the direction of the coordinate axis, x_1 being the main direction of propagation of the incident beam, x_2 being the normal to the plate and x_3 being along the plate and normal to x_1, as shown in Fig. 1. C_{ikjl} is the component of the complex stiffness tensor, ρ is the material density and ω ($2\pi f$) is the angular frequency. The above partial differential equation (PDE), Eq. (1), has been written in the following form imposed by the commercial software used in this study:

$$\nabla(c\nabla u) - au = 0,$$

where c is a 3×3 matrix. For an orthotropic material, axis of symmetry of which is coinciding with the coordinate axis, this matrix is composed by the following sub-matrices c_{kl}, where k, l = 1, 2, 3:

$$c_{11} = \begin{pmatrix} C_{11} & 0 & 0 \\ 0 & C_{66} & 0 \\ 0 & 0 & C_{55} \end{pmatrix}, \quad c_{12} = \begin{pmatrix} 0 & C_{12} & 0 \\ C_{66} & 0 & 0 \\ 0 & 0 & 0 \end{pmatrix},$$

$$c_{13} = \begin{pmatrix} 0 & 0 & C_{13} \\ 0 & 0 & 0 \\ C_{55} & 0 & 0 \end{pmatrix}, \quad c_{21} = \begin{pmatrix} 0 & C_{66} & 0 \\ C_{21} & 0 & 0 \\ 0 & 0 & 0 \end{pmatrix},$$

$$c_{22} = \begin{pmatrix} C_{66} & 0 & 0 \\ 0 & C_{22} & 0 \\ 0 & 0 & C_{44} \end{pmatrix}, \quad c_{23} = \begin{pmatrix} 0 & 0 & 0 \\ 0 & 0 & C_{23} \\ 0 & C_{44} & 0 \end{pmatrix},$$

$$c_{31} = \begin{pmatrix} 0 & 0 & C_{55} \\ 0 & 0 & 0 \\ C_{31} & 0 & 0 \end{pmatrix}, \quad c_{32} = \begin{pmatrix} 0 & 0 & 0 \\ 0 & 0 & C_{44} \\ 0 & C_{32} & 0 \end{pmatrix},$$

$$c_{33} = \begin{pmatrix} C_{55} & 0 & 0 \\ 0 & C_{44} & 0 \\ 0 & 0 & C_{33} \end{pmatrix}, \quad a = \begin{pmatrix} -\rho\omega^2 & 0 & 0 \\ 0 & -\rho\omega^2 & 0 \\ 0 & 0 & -\rho\omega^2 \end{pmatrix},$$

where C_{ij} are the material elastic or viscoelastic moduli, using the contracted notation and a is the above-defined 3×3 matrix.

Since this FE model consist in modeling the propagation in the frequency domain, absorbing regions (AR) must be used all around the plate to avoid unwanted reflections that would exist due to the permanent established dynamic regime. The definition of these 3D absorbing regions is based on a gradual increase of damping properties, as explained in Refs. [3] and [4]. The formula for absorbing region is as following:

$$C_{ij}^{AR} = C'_{ij}\left(1 + i * \left(\frac{Ra}{La}\right)^3\right) + i * C''_{ij}\,,\; C_{ij} = C'_{ij} + iC''_{ij}$$

Where Ra and La are the interval and length of absorbing regions respectively. The size of the AR used in this FE model is $1.5\lambda_{MAX}$, where λ_{MAX} is the maximum wavelength for all modes existing in the plate at the frequency of investigation. Since, the frequency of incident Lamb wave mode is below the one corresponding to A_1 cut-off, λ_{MAX} will be the wavelength of S_0 mode at the frequency of interest. This 3D FE model is already validated in [5].

3 Composite sample and schematic of the 3D FE model

The composite plate sample with average thickness 6.2 mm consists of 20 laminas of each 0.3 mm thick oriented in $[45/0/0/45/0/45/0/45/0/45]_S$ directions. The homogenized elastic moduli of the composite plate are shown in Table 1.

Table 1: Homogenized material properties of carbon fiber reinforced composite plate.

ρ (g/cm3)	C_{11} (GPa)	C_{22} (GPa)	C_{33} (GPa)	C_{12} (GPa)
1.55	52.4	12.6	52.4	3.15
C_{13} (GPa)	**C_{23} (GPa)**	**C_{44} (GPa)**	**C_{55} (GPa)**	**C_{66} (GPa)**
17.8	3.15	2.8	17.3	2.8

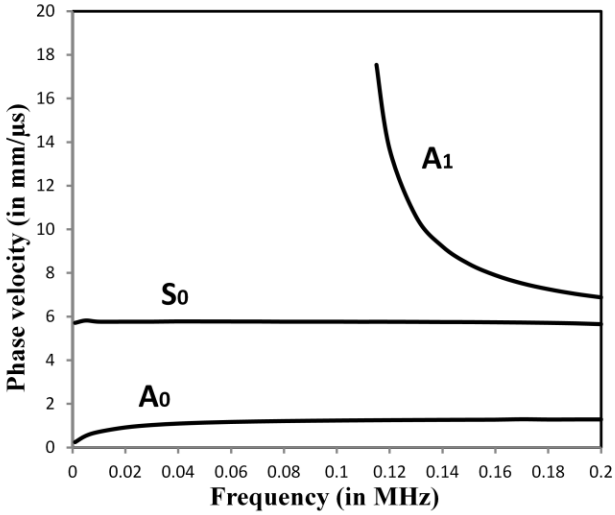

Figure 1: Phase velocity dispersion curves for the composite plate sample.

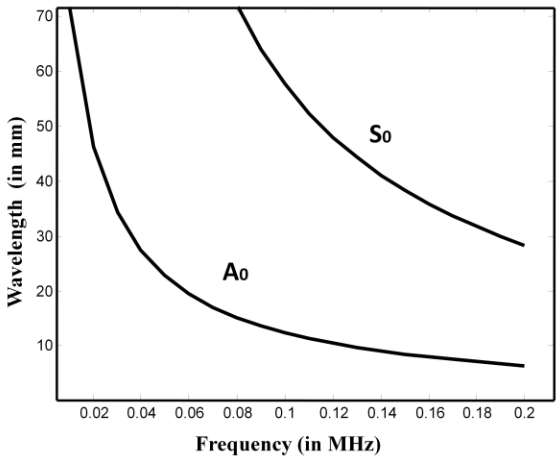

Figure 2: Wavelength dispersion curves for the composite plate sample.

An equal proportion of 5% of each respective real elastic constant is considered as imaginary part of the elastic constants to include the effective damping in the material. The dispersion curves corresponding to phase velocity and wavelength versus frequency are plotted using SAFE (Semi Analytic Finite Element) method for this composite plate sample and shown in Fig. 1 and Fig. 2.

It is observed that after 120kHz, higher wave mode A_1 starts to appear in the dispersion curves. So, we have chosen the excitation frequency (f) equal to 100 kHz for this study to avoid higher order Lamb wave modes. At this frequency of 100 kHz, the wavelengths of A_0 and S_0 modes are 12.4 mm and 57.7 mm, respectively. So the size of the AR is about 87 mm all around the four sides of the FE model. The diameter of the circular regions (i.e. PZT disks) used in this model is 20 mm wide for the excitation purpose. Considering the above mentioned arguments and computation time for solving the model, we considered the face of composite plate as square with 300 mm length. The excitation is placed on the both faces of the plate with center at a point (110, y, 110). The conical shaped damaged zone is placed first at the center of the plate being tip of the cone at the surface of the plate at (150, 6.2, 150) and then at a point at (175, 6.2, 150) making incident angle with defect as 225° and 238° respectively. The monitoring positions for the normal displacement at the mid plane around the conical defect is at a distance of 20 mm as shown with white dots around damage. The schematic of the 3D-FE model is shown in Fig. 3.

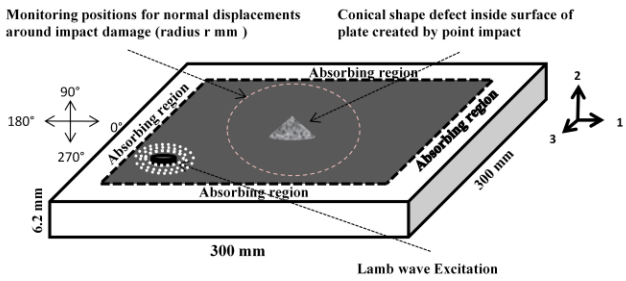

Figure 3: Schematic of 3D-Finite Element model.

4 Impact damage shape and modeling in Composite 3D-FE model plate

For our study, it is assumed that the material is strongly micro-cracked inside the impact damage zone and the shape of this zone is supposed to be that of a right circular cone due to transversely isotropic nature of the plate. In three dimensions, we assume that a uniform point impact would produce a damage zone, the shape of which would be a right circular cone. So, the cracked zone inside the composite plate is modeled as a right circular cone with height of the cone as depth *(d)* of the damage and radius *(r)* of the base of the circle as conical width of the damage zone. In the FE model, we represent this cracked zone by 80% decrease in the material stiffness, in the real part of $C_{ij,}$ regarding the imaginary parts of the moduli, their proportions relative to the real parts are kept unchanged. The choice of 80% decay in the material stiffness rather than other smaller value is motivated by the fact that the damaged zone in FE model is considered as a homogeneous medium with mass density equal to that of undamaged material, although it would likely be a heterogeneous region made of cracks, voids and delaminations, which are known to be efficient scatterers of elastic waves. In a previous study [6], it is seen that an 80% value is quite representative of a severely cracked and delaminated zone, in terms of wave scattering.

5 Interaction of A_0 mode with impact damage

At first, a 3D-FE model is constructed which includes no defect. This model is then used for calculating the incident field of A_0 wave mode. For this purpose, the model is constructed with the same properties and dimensions as mentioned in section 3 of the paper. The excitation of pure A_0 Lamb wave mode is introduced at a point (110,0,110) and (110,6.2,110) as centre with 20 mm diametric circular area (PZT circular disks) and giving unit normal stress in same direction on both faces of the plate. Lagrange-quadratic hexahedral elements with maximum element size equal to λ_{min} /4 are used, where $\lambda_{min} = \lambda_{A0} \approx$ 12.4 mm, i.e. 3 mm has been chosen as maximal element size. The whole model contains a total of 30,000 hexahedral elements, and 8,48,421 degrees of freedom. Preliminary convergence tests have been carried out to ensure good level of accuracy of numerical predications. The model is solved at a frequency of 100 kHz and applying stress-free boundary conditions all around the six faces of the plate using Neumann boundary conditions. After solving the model, out-of-plane displacements *v* at mid plane (y= 3.1 mm) are monitored in circular positions on the 360 points around the center (150, 3.1, 150) at a radius distance of 20 mm. The absolute amplitude of incident A_0 mode is shown in a polar plot in Fig. 4. The incident angle for such configuration is 225°. We observe that the incident amplitude of A_0 mode is perfectly symmetric along 225°-45° due to the transversely isotropic nature of the plate along Y-axis.

Case I: In the first case, a right circular conical defect with tip at the surface at (150, 6.2, 150) of the plate are inserted in the FE model. The dimensions of this conical impact damaged zone are set as depth *d* equal to 5.1 mm and radius of the base *r* equal to 15 mm (larger than the wavelength 12.4 mm of incident A_0 mode) for the study. The reason for considering such dimensions of the damage is that we have observed these values in actual experimental on the sample plate with a point impactor having energy of the impact equal to 40 Joules. However, this article deals only with numerical predictions of scattering phenomenon. The same choice of maximal element size of 3 mm is implement as used earlier for incident field. The model contains 1,84,706 tetrahedral elements with 9,63,414 degrees of freedom. The element size is not changed in the vicinity of the damaged zone considering computational limitation of the computer machine; therefore small errors might occur in the near field due to the inaccurate description of the stress concentration. The same frequency of 100kHz is used to solve the model with Neumann boundary conditions and normal displacements *v* at mid plane (y= 3.1 mm) are monitored in circular positions around the center (150, 3.1, 150) at a same radial distance of 20 mm. The absolute total wave field with A_0 incident mode due to damage is shown in a polar plot in Fig. 5. A snapshot of real part of total out-of-plane displacements at mid plane of the plate is shown in Fig 6.

Figure 4: Polar plot of incident amplitude of A_0 mode at mid plane (monitored at 20 mm radius); incident wave angle = 225°; *f* = 100 kHz; λ = 12.4 mm.

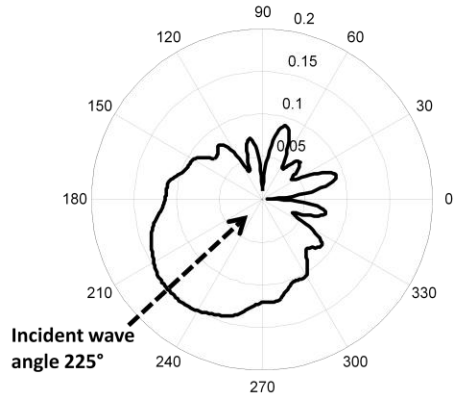

Figure 5: Polar plot of total wave field of A_0 incident mode due to damage at mid plane (monitored at 20 mm radius); incident wave angle = 225°; *f* = 100 kHz; λ = 12.4 mm; diameter of base of damaged zone = 15 mm.

The amplitude of wave scattered at impacted zone is calculated as difference between the complex magnitudes for each point with and without a defect. The normalized

scattered amplitude of A_0 mode is shown in Fig. 7. It is clear from the Fig. 7 that the total wave field is also perfectly symmetric along 225°-45° due to the transversely isotropic nature of the plate along Y-axis. The maximum amplitude of the scattered A_0 wave mode is towards the 45°. The normalized amplitude of A_0 mode does not change much along 180° towards 300° and it is almost negligible near 30° and 60°. So, the possibility of detecting A_0 mode along 30° and 60° will be very less as compared to other directions.

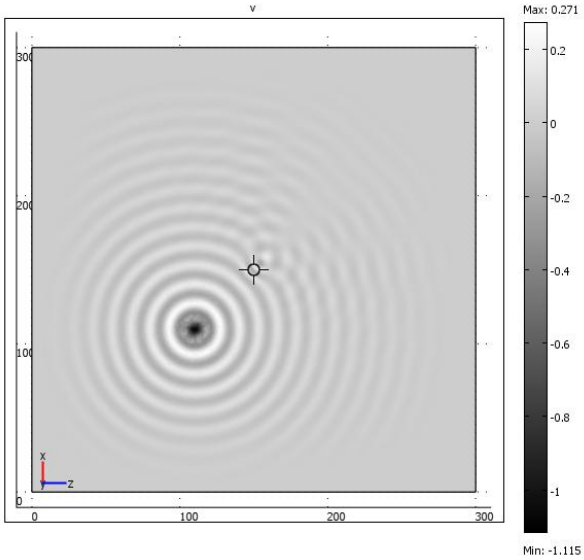

Figure 6: Real part of total wave field at mid plane with defect; incident wave angle = 225°; f = 100 kHz; λ = 12.4 mm; diameter of base of damaged zone = 15 mm.

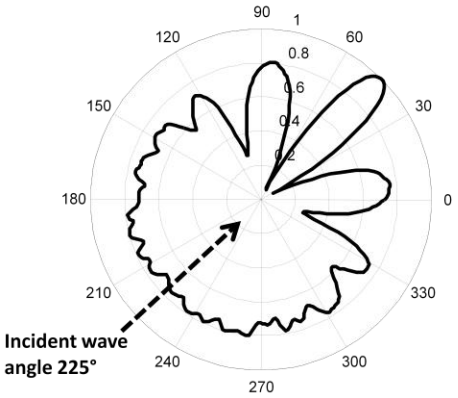

Figure 7: Polar plot of normalized amplitude of A_0 mode scattered at damaged zone (monitored at 20 mm radius); incident wave angle = 225°; f = 100 kHz; λ = 12.4 mm; diameter of base of damaged zone = 15 mm.

Case II: In the second case, the same right circular conical defect with tip at the surface at (175, 6.2, 150) of the plate are inserted in the FE model. The positions of incident wave mode are same as before. Due to this, the angle of incident A_0 mode towards the defect is around 238°. This model contains 1,84,307 tetrahedral elements with 9,60,765 degrees of freedom. The same procedure is followed around the damage to calculate the scattered amplitude of A_0 mode. The polar plot of normalized scattered amplitude of A_0 mode is shown in Fig. 8. The maximum amplitude of the scattered A_0 wave mode is towards the 58° and the normalized amplitude does not change much along 180° towards 300°. Almost same pattern is observed as we have seen in 225° of incidence. A little asymmetry is observed in this figure along 238°- 58° direction, this may be due to small numerical errors in the computations.

6 Variation of scattered field due to defect geometry size

In this section, we have plotted the scattering directivity diagrams with respect to different size of the base of the conical impact damage and with different height of the conical damaged zone. The position for incident A_0 mode and the position for the tip of the conical damage is considered same as in Case I discussed above. Four different diameter (2r) of the conical zone considered are as 10 mm, 20 mm, 30 mm and 40 mm. The absolute normalized scattered amplitude of A_0 mode for different base diameters are shown in Fig. 9. For first three radii (5 mm, 10 mm and 15mm), the normalized amplitudes are very close to each other between 150° and 300° (anti-clock wise). The normalized amplitude for 20 mm radius is almost 50% of the remaining cases, but the shape remains almost same. These all four cases are almost symmetrical towards incident angle of 225° along 45°. Between 150° and 300° (clock wise), in all four cases amplitudes behave differently. For radii 10 mm and 15 mm, the maximum amplitude of scattered wave is towards 45°, but very small for radii equal to 5 mm and 20 mm in 45° direction.

In Fig. 10, we have seen the effect in directivity pattern with variations of different heights of conical damage as ¼, ½, ¾ and all through thickness of plate thickness of 6.2 mm considering the base diameter of damage equal to 30 mm wide. In all four cases, there is scattering in 45° direction. For ½ and ¾ depth of the zone, the amplitude is maximum towards 45° direction. For full and ¼ of depth of the zone, between 150° and 300° (clock wise) the amplitudes are almost same. Between 150° and 300° (clock wise), in all four cases amplitudes behave differently as in earlier case. In both cases, the directivity diagrams are found to be almost symmetrical along 225°-45° direction.

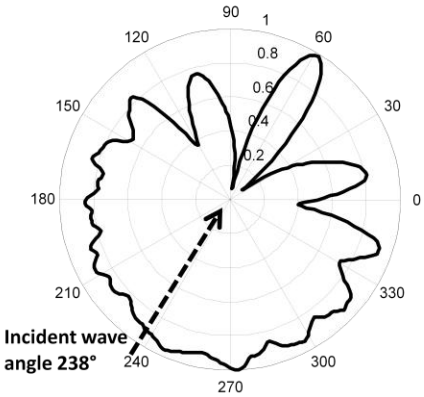

Figure 8: Polar plot of normalized amplitude of A_0 mode scattered at damaged zone (monitored at 20 mm radius); incident wave angle = 238°; f = 100 kHz; λ = 12.4 mm; diameter of base of damaged zone = 15 mm.

7 Conclusion

A 3-Dimensional Finite Element numerical study have been performed for computing the scattering behaviour of A_0 lamb mode with a point impact damage in the plate. The point impact damage inside the plate is modeled as a right circular conical geometry with 80% decay in material stiffness while density remaining the same as undamaged state. Two different positions of impact damage relative to

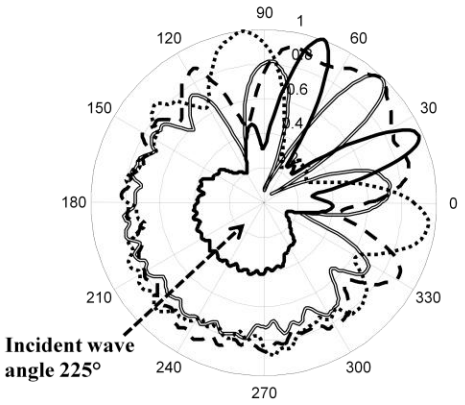

Figure 9: Polar plot of normalized amplitude of A_0 mode at mid plane (monitored at 20 mm radius); incident wave angle = 225°; f = 100 kHz; λ = 12.4 mm; height h = 5.2 mm; radius r of base of damaged zone = 5mm (**.....:** dotted line); 10mm (- - - -: dashed line); 15mm (===: double line); 20mm (**____:** solid line).

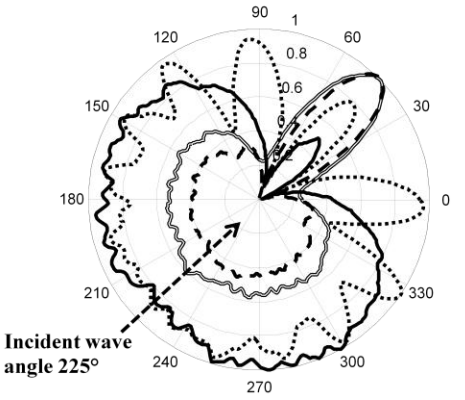

Figure 10: Polar plot of normalized amplitude of A_0 mode at mid plane (monitored at 20 mm radius); incident wave angle = 225°; f = 100 kHz; λ = 12.4 mm; radius r = 15 mm; height h of conical damaged zone = 6.2mm (**.....:** dotted line); 4.65mm (- - - -: dashed line); 3.1mm (===: double line); 1.55mm (**____:** solid line).

angle of incident of A_0 mode is studied. Also, the effect of geometric size of the damaged zone is presented in the scattering diagrams. It is observed that the maximum normalized scattered amplitude of A_0 mode is towards angle of incidence direction for the case of depth and radius of 5.1 mm and 15 mm respectively. The change in scattered amplitude for different base radii of the damage is very small in 150°-300° anti-clock wise direction while directivity of amplitude changes much in 150°-300° clock wise direction. In the case of different depths of the impact damage the amplitude of the scattered wave are different in 150°-300° anti-clock wise direction while towards 45° there is always a potion of scattered wave with different amplitudes. In all the different cases of depths, there are angles near 30° and 60° where a very negligible amplitude of scattered A_0 mode is observed. The study presented in this paper may give an idea for permanent placements of PZT sensors for structural health monitoring of composite structures.

The future work will be the comparisons of numerical results with the experimental measurements for a real point impact damage on composite plate sample provided by DAHER-SOCATA, France.

Acknowledgments

The work has been supported by the project ECOWINGBOX.

References

[1] Seale MD, Madaras EI. Ultrasonic measurements of stiffness in thermal– mechanically fatigued IM7/5260 composites. J Mater Eng Perform 1999; 8(4):429–36.

[2] COMSOL, User's Guide. Version 3.5a by COMSOL AB 2008 〈http://www.comsol.com/〉, (last viewed 30th January 2012).

[3] Drozdz M. Efficient Finite Element modelling of ultrasound waves in elastic media. PhD theses, Mechanical Engineering, Imperial College London, 2008.

[4] Drozdz M, Lowe M, Cawley P, Moreau L, Castaings M. Efficient numerical modeling of absorbing regions for boundaries of guided waves problems. In: Thompson DO, Chimenti DE. Editors. Review of progress in quantitative non destructive evaluation, AIP Conference Proceedings, New York, 25A, p. 126–33, 2006.

[5] Ke W, Castaings M, Bacon C, 3D finite element simulations of an air-coupled ultrasonic NDT system. NDT & E International 2009; 42: 524-533.

[6] Castaings M, Singh D, Viot P, Sizing of impact damages in composite materials using ultrasonic guided waves. NDT & E International 2012; 46: 22-31.